Thermal Antibubbles: When Thermalization of Encapsulated Leidenfrost Drops Matters

Jonas Miguet, Benoit Scheid, Laurent Maquet, Baptiste Darbois Texier, Stéphane Dorbolo

Thermal Antibubbles: When Thermalization of Encapsulated Leidenfrost Drops Matters

Jonas Miguet,[1] Benoit Scheid,[1,*] Laurent Maquet,[2] Baptiste Darbois Texier,[2,3] and Stéphane Dorbolo[2]
[1]*TIPs, Université Libre de Bruxelles, CP 165/67, Brussels, Belgium*
[2]*GRASP, CESAM, Université de Liège, Liège, Belgium*
[3]*Université Paris-Saclay, CNRS, FAST, 91405 Orsay, France*

(Received 17 April 2023; accepted 20 September 2023; published 30 October 2023)

Antibubbles are ephemeral objects composed of a liquid drop encapsulated by a thin gas shell immersed in a liquid medium. When the drop is made of a volatile liquid and the medium is superheated, the gas shell inflates at a rate governed by the evaporation flux from the drop. This thermal process represents an alternate strategy for delaying the antibubble collapse. We model the dynamics of such "thermal" antibubbles by incorporating to the film drainage equation the heat-transfer-limited evaporation of the drop, which nourishes the gas shell with vapor, as for Leidenfrost drops. We demonstrate that the inflation of the gas shell is drastically inhibited by the thermalization of the initially colder drop. Because of this thermalization effect, smaller drops evaporate much faster than larger ones.

DOI: 10.1103/PhysRevLett.131.184001

An antibubble is a unique object, which owns its name for being the contrary of a soap bubble [1–3]. If a soap bubble is a thin spherical shell of soapy liquid surrounded by air, an antibubble is a thin spherical shell of air surrounded by soapy liquid. In a recent paper [4] we reviewed the various factors controlling the lifetime of antibubbles with surfactants, envisioning the feasibility of future applications requiring a fine control of the lifetime, like for instance in enhancing ultrasonic imaging [5,6], or in oil-free encapsulation and drug vectorization [7]. Creating antibubbles without surfactant is much more challenging, and their lifetimes are dramatically reduced, i.e. from minutes to fractions of seconds, such that they can hardly be observed without the help of high-speed imaging. Yet, surfactant-free antibubbles can be obtained by impacting a viscous drop onto a gas-liquid interface [8]. Under certain size and impact speed conditions, the drop does not coalesce and rather entrains some gas layer below the interface. The gas layer encapsulates the drop and the antibubble forms. There, delayed-coalescence relies on the viscous resistance of the intervening gas layer during the impact. Now, the coalescence of the drop with the bath can be delayed even longer if the intervening gas layer is additionally fed with vapor. This strategy was reported in the 1960s by Hickmann to obtain the so-called *boules* of liquid floating above the same superheated liquid [9], and later associated to the Leidenfrost effect [10] in the particular case of a drop of a volatile liquid gently released on a hot liquid bath [11]. In the 1980s, by releasing the drop with higher impact speed, Ida and Takashima [12] and Nosoko and Mori [13] succeeded to form *thermal antibubbles*, without naming it, but instead referring to *submerged film boiling*. In this Letter, we revisit this thermal antibubble regime [12,13] as sketched in Fig. 1, and demonstrate that the inflation of the gas shell due to the production of vapor is strongly limited by the thermalization of the initially colder drop.

Despite decades of studies on the Leidenfrost effect, which threatens the safety of several industrial installations, the prediction of the onset of this phenomenon remains poorly understood. One of the issues that remains to be

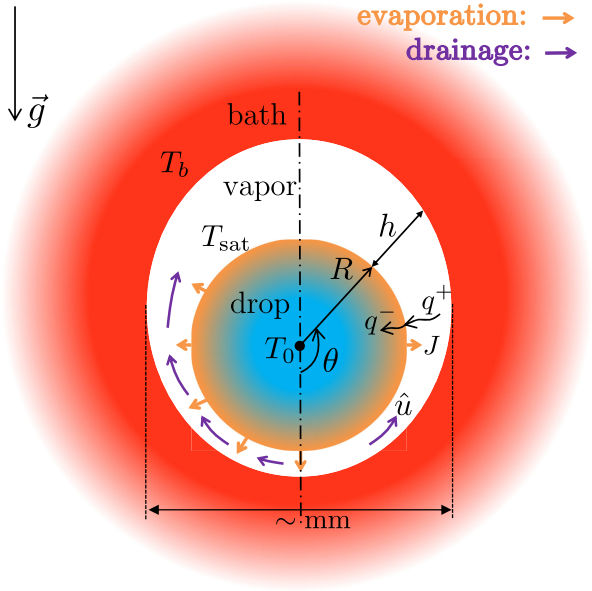

FIG. 1. Thermal antibubble: the heat provided by the hot bath is used for both evaporating and thermalizing the initially cold drop. The generated vapor, while draining from bottom to top, delays the antibubble collapse.

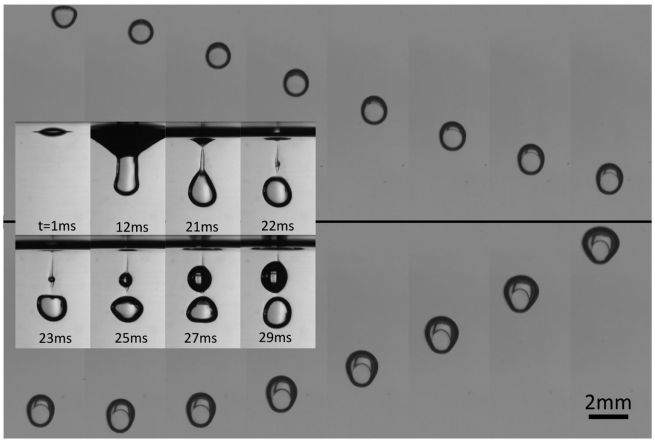

FIG. 2. Snapshot series every 24 ms presenting the motion of a thermal antibubble made of an HFE-7100 droplet released into a bath of V20 silicone oil heated at $T_b = 120\,°\mathrm{C}$. The change of direction occurs 203 ms after the first image, i.e. between the ninth and the tenth snapshots. Inset: snapshot series presenting the formation of the thermal antibubble in the same conditions. A satellite thermal antibubble is seen to be formed within the "tail" of the main one. The scale bar applies to all snapshots.

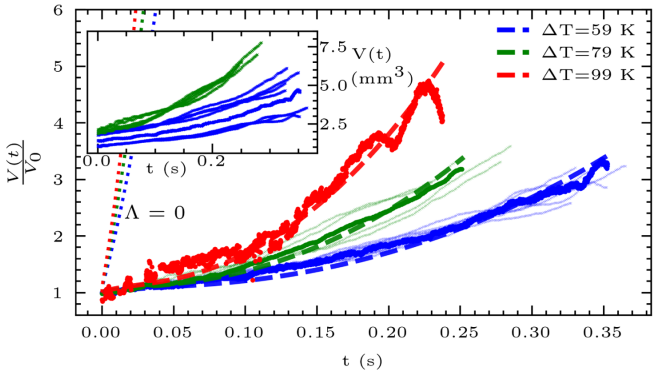

FIG. 3. Normalized thermal antibubble volume as a function of time for different ΔT. Thick dashed lines represent the model output, adjusted to the particular experiment represented with filled circles. The thin crosses correspond to additional experiments. Thick dotted lines are the model output without the thermalization term ($\Lambda = 0$). Inset: all of the non-normalized experimental data for $\Delta T = 59$ and 79 K.

investigated is the transient dynamics of the Leidenfrost effect, a study that is highly challenging from a technical point of view. Recent advances in experimental techniques have made it possible to characterize this transient dynamics [14–17]. However, these observations on the onset of the Leidenfrost state should now be rationalized, and thermalization should be an essential ingredient in this problem. Thermalization has only been considered in inverse Leidenfrost systems [18,19], for which the heat reservoir for evaporating the bath surface is limited by the size of the hotter drop, while for the direct Leidenfrost system, the heat reservoir for evaporating the drop is usually not limited by the size of the bath. Yet, a significant part of the heat flux coming from the bath to evaporate the drop is hijacked at the first instants for thermalizing the initially colder drop. Thermal antibubble therefore constitutes a unique system allowing one to quantify the vapor generated by a (direct) Leidenfrost droplet and assess the role of thermalization in the Leidenfrost onset.

In our experimental procedure, a bath made of V20 silicone oil is heated at a temperature T_b higher than the saturation temperature $T_{\mathrm{sat}} = 61\,°\mathrm{C}$ of the drop made of hydrofluoroether 7100 (HFE). The drop, initially at the ambient temperature $T_0 = 25\,°\mathrm{C}$, is released at the appropriate height to obtain antibubbles [13,20]. An example of antibubble formation, obtained with a high speed camera, is depicted in the inset of Fig. 2. The drop of radius $R = 760\ \mu\mathrm{m}$ impacts the bath with a speed $U_0 = 0.56\ \mathrm{m/s}$ that provides sufficient kinetic energy for the drop to cross the interface and form a cylindrical cavity. The cavity pinches off at about 20 ms after the impact due to the Rayleigh-Plateau instability [21], such as the impacting drop is encapsulated by an air shell, forming a thermal antibubble. A satellite antibubble is also formed in this case, and is seen to grow considerably faster than the main antibubble, a size-dependent behavior that will be rationalized in this Letter.

Thermal antibubbles are only obtained for a specific range of impact speeds, which varies with the superheat $\Delta T = T_b - T_{\mathrm{sat}}$. The corresponding phase diagram appears to be nonuniversal [22], hence different than the one found by Nosoko and Mori [13] for a drop of fluorocarbon refrigerant R113 into a bath of ethylene glycol. Typical evolution of the thermal antibubble after its formation is also shown in Fig. 2. It first sinks because the density ρ_d of HFE is larger than the density ρ_b of the oil. Then, the generation of HFE vapor in the antibubble implies the inflation of the time-dependent antibubble volume $V(t)$, hence the decrease of the antibubble downward velocity down to the point it becomes neutrally buoyant. Neglecting the vapor density as compared to the liquid densities, this buoyancy match gives the following volume ratio $V/(\frac{4}{3}\pi R^3) \approx \rho_d/\rho_b = 1.72$, as verified experimentally at $t = 203$ ms for which the antibubble changes direction [22]. Next, the buoyancy force becomes larger than the weight of the remaining HFE drop, and the antibubble goes back up. Eventually, the antibubble ends its life by popping up at the free surface of the bath.

Figure 3 presents the time evolutions of antibubble volume for three superheats, i.e. $\Delta T = 59$, 79 and 99 K, and different initial radii (see inset for the non-normalized data). The volume was reconstructed by assuming that the antibubbles were axisymmetric. The initial antibubble volume $V(0) = V_0$ was determined by averaging the antibubble volume over the first 5 ms, to smooth out the variability intrinsic to the antibubble deformations right after the pinch-off. When the antibubble volume is

normalized by the initial volume, the volume inflation rate clearly increases with increasing ΔT, despite the dispersion of the data that comes from variations in the velocity of the drop into the bath [22], and most importantly from variations of the drop radius, a dependence that is explained below. Filled circles data points for each ΔT in Fig. 3 are those corresponding to a representative mean radius, chosen for fitting the model.

We model the thermal antibubble by assuming the vapor shell to drain axisymmetrically along the polar coordinate θ, whose origin is taken at the bottom of the antibubble. Because of the large contrast of density between the vapor and the liquid drop, it is assumed that the radius of the drop remains constant during the time the thermal antibubble takes to reach the surface of the liquid bath. As sketched in Fig. 1, $h(\theta, t)$ is the thickness of the vapor film, $\hat{u}(\theta, t)$ is the average vapor velocity over the film thickness, and $J(\theta, t)$ is the evaporation mass flux from the drop, t being the time. The conservation equation for the flow in the vapor film then reads

$$\partial_t h + \nabla \cdot (h\hat{u}) = \frac{J}{\rho_v}, \tag{1}$$

where ∂_t is the partial derivative operator with respect to t, ∇ is the nabla operator, and ρ_v is the vapor density. The local evaporation flux at the interface is expressed as

$$J = -\frac{q^+ - q^-}{\mathcal{L}}, \tag{2}$$

where $\mathcal{L}$ is the latent heat of vaporization, q^+ is the heat flux brought by the bath through the vapor film at the drop surface, while q^- is the heat flux lost to thermalize the drop, initially at the ambient temperature T_0.

First, the average velocity is obtained in the frame of the lubrication theory, valid for $h/R \ll 1$, as performed in [31] for isothermal antibubbles. Assuming no-slip at the liquid/vapor interfaces, as commonly considered in Leidenfrost problems (see e.g. [11]), it yields

$$\hat{u}(\theta, t) = -\frac{h^2}{12\mu_v R}\partial_\theta p, \tag{3}$$

where μ_v is the dynamic viscosity of the vapor, and

$$\partial_\theta p = -\rho_d g R \sin\theta - \gamma_b \partial_\theta (\nabla \cdot \nabla h) \tag{4}$$

is the pressure gradient governing the drainage of the vapor, g being the gravitational acceleration, and γ_b the interfacial tension of the oil-vapor interface. The first term in (4) represents the hydrostatic pressure difference along the film and the second one represents the capillary pressure gradient due to deformations of the outer interface—the sphericity of the inner interface being ensured by the excess of Laplace pressure inside the drop.

Second, the heat transfer in the vapor film is assumed to be purely conductive, implying a constant temperature gradient $\Delta T/h$ across the vapor film, as commonly used in Leidenfrost problems (see e.g. [11]), such that

$$q^+ = -k_v \frac{\Delta T}{h}, \tag{5}$$

with k_v the thermal conductivity of the vapor. Note that the constant temperature at the bath interface is ensured by the convective heat transfer induced by the buoyant motion of the antibubble into the bath [22].

Third, the heat transfer in a spherical drop with a constant surface temperature has an analytical solution in the form of error-function series [23], which converges rapidly at short time, namely for $t \ll \tau_d$, where $\tau_d = R^2/\chi_d$ is the diffusion timescale in the liquid drop and χ_d is its thermal diffusivity. The temperature gradient at the drop surface can thus be straightforwardly obtained by deriving once the solution given in [23] truncated at the first term, yielding [22]

$$q^- = -k_d \frac{\Delta T_d}{R}\left(\sqrt{\frac{\tau_d}{\pi t}} - 1\right), \tag{6}$$

with $\Delta T_d = T_{\text{sat}} - T_0$, and k_d is the thermal conductivity of the liquid drop.

Combining Eqs. (2)–(6) with (1), scaling h with the initial uniform film thickness h_0, t with the viscous-gravity drainage time $\tau = \mu_v R/(\rho_d g h_0^2)$, and writing the divergence operator in spherical coordinates, finally lead to the dimensionless time-evolution equation of the vapor shell nourished by the evaporation flux:

$$\partial_{\bar{t}}\bar{h} + \frac{1}{\sin\theta}\partial_\theta\left[\sin\theta\frac{\bar{h}^3}{12}\left\{\sin\theta + \frac{1}{\text{Bo}}\partial_\theta\left(\frac{1}{\sin\theta}\partial_\theta(\sin\theta\partial_\theta\bar{h})\right)\right\}\right] = E\left\{\frac{1}{\bar{h}} - \Lambda\left[\frac{1}{\sqrt{\pi\text{Fo}(\bar{t}+\bar{t}_c)}} - 1\right]\right\}, \tag{7}$$

where bars denote dimensionless variables, and where the dimensionless numbers are defined as follows:

$$\text{Bo} = \frac{\rho_d g R^3}{\gamma_b h_0}, \quad E = \frac{k_v \mu_v R \Delta T}{\rho_v \rho_d g \mathcal{L} h_0^4}, \quad \Lambda = \frac{k_d h_0 \Delta T_d}{k_v R \Delta T}, \quad \text{Fo} = \frac{\tau}{\tau_d}.$$

The Bond number Bo quantifies the capillary pressure effect as compared to the hydrostatic pressure difference driving the drainage, i.e. $2R\rho_d g$. The evaporation number E represents the dimensionless evaporation rate. The thermalization number Λ compares the heat flux directed to the drop with the heat flux coming from the bath. The Fourier number Fo compares the drainage timescale in the film to the thermal diffusion timescale in the drop. Notice that the validity of the thermalization heat flux in (7) is ensured as

TABLE I. Values of the parameters used in this work. Properties for the liquid drop (index d) are those for HFE-7100 at T_0 [32]. Properties for the vapor (index v) are those for HFE-7100 at average temperature $T_{\text{sat}} + \Delta T/2$ [24]. Properties of the bath (index b) are those for silicone oil V20 at T_b [33]. See Ref. [22] for details on the temperature dependence of parameters.

Fixed parameters:		T-dependent parameters:			
T_{sat} (°C)	61	T_b (°C)	120	140	160
T_0 (°C)	25	ΔT (K)	59	79	99
ΔT_d (°C)	36	γ_b (mN/m)	15	14	13
$\mathcal{L}$ (kJ/kg)	112	ρ_v (kg/m^3)	8.38	8.15	7.94
k_d (mW/K/m)	69	μ_v (μPa s)	14.3	15.2	16.0
ρ_d (kg/m^3)	1510	k_v (mW/K/m)	*13.8*	*14.7*	*15.5*
χ_d (mm^2/s)	0.04	$k_{v_{\text{fit}}}$ (mW/K/m)	**13.2**	**14.4**	**12.7**
Measured parameter:		V_0 (μl)	1.41	2.03	1.07
Calculated parameter:		R (μm)	692	781	630
Dimensionless numbers:		Fo($\times 10^{-3}$)	3.4	3.2	4.1
		Bo($\times 10^{1}$)	8.2	12.6	7.1
		Λ($\times 10^{-2}$)	1.8	1.1	1.3
		E($\times 10^{3}$)	2.2	3.9	3.8

long as Fo $\ll 1$, which is verified in Table I. The novelty in Eq. (7) holds in the incorporation of the drop thermalization heat flux gauged by Λ. A dimensionless offset time $\bar{t}_c = t_c/\tau$ is necessary to regularize the thermalization term that diverges at $\bar{t} = 0$. We set $t_c = 1$ ms for all computations, which has been found to be small enough to have no influence on the results [22]. For the initial uniform film thickness, we set $h_0 = 4$ μm, corresponding to the average thickness for isothermal antibubbles [4]. The drop radius was then calculated as $R = \sqrt[3]{3V_0/4\pi} - h_0$. Equation (7) is closed with symmetry conditions imposed at each pole, i.e. $\partial_\theta \bar{h} = \partial_{\theta\theta\theta}\bar{h} = 0$ at $\theta = \{0, \pi\}$, and with $\bar{h} = 1$ as the initial condition. The model has been solved using COMSOL Multiphysics with fixed and temperature-dependent parameters given in Table I. The time evolution of the antibubble volume has been reconstructed from the solution $\bar{h}(\theta, t)$ using

$$V(t) = \frac{2}{3}\pi R^3 \int_0^\pi \left(1 + \frac{h_0}{R}\bar{h}\right)^3 \sin\theta \, d\theta. \tag{8}$$

Results in thick dashed line in Fig. 3 show that the experimental trend is recovered with the model. The volume increase is accelerated with respect to a purely diffusion-limited growth (that should result in a square-root dependence of the volume to time [22]), which is a signature of the drainage: as the vapor drains upwards, the film thins at the bottom, increasing the evaporation flux $\propto 1/\bar{h}$. The modeling curves correspond to our best fits using the thermal conductivity of the vapor phase k_v as the fitting parameter, and denoted $k_{v_{\text{fit}}}$ in Table I (values in bold). Each fit is obtained by minimizing the root mean square difference between the experimental curve and the modeling curve for varying k_v. Note that for a given ΔT, the fitting has only been applied to one of the experimental curves chosen to have a representative radius. The rationale behind our fitting approach is that k_v is not precisely known *a priori* as it is sensitive to temperature. Yet, the fitting values $k_{v_{\text{fit}}}$ are very close to the values taken at the mean temperature $T_{\text{sat}} + \Delta T/2$ as usually considered in Leidenfrost problems (see the italic values for k_v in Table I), which is a good indication that the model represents the system correctly at leading order. This is confirmed in Fig. 3 where the modeling curves have been plotted in absence of thermalization, i.e. for $\Lambda = 0$, and depict an order-of-magnitude faster volume growth than in the experimental cases. It is actually found that approximately 95% of the heat provided by the conductive flux between the bath and the droplet is pumped by the latter in the form of sensible heat. These results demonstrate the predominance of thermalization effect for systems featuring lifetimes well below the diffusive timescale τ_d. This is further evidenced by observing the evolution of the satellite antibubble formed at pinch-off, as observed in the last five snapshots of the inset of Fig. 2 for $\Delta T = 59$ K, where the satellite antibubble is seen to inflate about 50 times faster than the main antibubble, meaning that the same amount of vapor produced in 7 ms for the satellite is produced in about 360 ms for the main antibubble. Since the initial radius for this satellite is one order of magnitude smaller than the radius of the main antibubble, the thermalization arises two orders of magnitude faster, such that the evaporation is also at least one order of magnitude more intense, as it is much less hindered by the drop thermalization effect. The influence of the antibubble size is illustrated in Fig. 4 that shows the computed volume inflation for $\Delta T = 79$ K and $k_v = 14.4$ mW/m/K for different initial radii. The volume growth measured for a main antibubble of 787 μm radius and a satellite antibubble of 118 μm radius are superimposed to the modeling curves. The model is thus shown

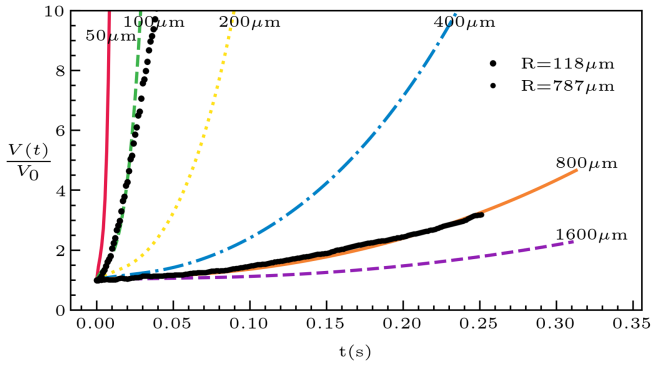

FIG. 4. Evolution of the thermal antibubble volume computed for $\Delta T = 79$ K, $k_v = 14.4$ mW/m/K, and varying initial radius. Symbols are experimental results for two different radii.

to rationalize the size dependence of the volume inflation thanks to the thermalization term.

To conclude, we presented surfactant-free thermal antibubbles relying on the vapor feeding of the gas shell given that the liquid bath temperature is higher than the saturation temperature of the liquid drop. We implemented an additional term in the classical film equation for Leidenfrost problems to account for the thermalization of the evaporating liquid drop. We then demonstrated that this term is essential to quantitatively compare with the experimental data when the drop is initially cold and that the transient matters, namely, that the observation timescale is smaller than the thermal diffusion timescale τ_d in the encapsulated Leidenfrost drop. For a radius of 700 μm, it corresponds to 10 s, but for a radius of 100 μm, it would only be 100 ms. Inversely, by suppressing the thermalization term, we found that the evaporation rate increases by at least an order of magnitude. Thermal antibubbles are therefore shown to be unique in monitoring the evaporation rates and thermalization effects of encapsulated volatile drops under various thermal conditions, as enabled by a direct visualization of their inflating volumes.

We thank Benjamin Sobac and Alex Rednikov for useful discussions on the Leidenfrost effect. Prof. N. Vandewalle is thanked for the use of GRASP facilities. This research has been funded by the Inter-university Attraction Pole Program (IAP 7/38 MicroMAST) initiated by the Belgian Science Policy Office. L. M. thanks ESA-BELSPO (PRODEX projects) for financing this research. J. M., B. S., and S. D. gratefully acknowledge financial support of the F. R. S.-FNRS through the PDR-STABAB project.

*Benoit.Scheid@ulb.be

[1] W. Hughes and A. R. Hughes, Nature (London) **129**, 59 (1932).
[2] C. L. Stong, Sci. Am. **230**, No. 4 116 (1974), https://www.jstor.org/stable/24950058.
[3] S. Dorbolo, H. Caps, and N. Vandewalle, New J. Phys. **5**, 161 (2003).
[4] Y. Vitry, S. Dorbolo, J. Vermant, and B. Scheid, Adv. Colloid Interface Sci. **270**, 73 (2019).
[5] M. Postema, F. J. ten Cate, G. Schmitz, N. de Jong, and A. van Wamel, Lett. Drug Des. Discovery **4**, 74 (2007).
[6] S. Kotopoulis, K. Johansen, O. H. Gilja, A. T. Poortinga, and M. Postema, Acta Phys. Pol. A **127**, 99 (2015).
[7] J. E. Silpe and D. W. McGrail, J. Appl. Phys. **113**, 17B304 (2013).
[8] D. Beilharz, A. Guyon, E. Li, M. Thoraval, and S. Thoroddsen, J. Fluid Mech. **779**, 87 (2015).
[9] K. Hickman, J. Maa, A. Davidhazy, and O. Mady, Ind. Eng. Chem. **59**, 18 (1967).
[10] D. Quéré, Annu. Rev. Fluid Mech. **45**, 197 (2013).
[11] L. Maquet, B. Sobac, B. Darbois-Texier, A. Duchesne, M. Brandenbourger, A. Rednikov, P. Colinet, and S. Dorbolo, Phys. Rev. Fluids **1**, 053902 (2016).
[12] Y. Iida and T. Takashima, Int. J. Heat Mass Transfer **23**, 1263 (1980).
[13] T. Nosoko and M. H. Mori, J. Heat Transfer **107**, 385 (1985).
[14] G. C. Lee, H. Noh, H. J. Kwak, T. K. Kim, H. S. Park, K. Fezzaa, and M. H. Kim, Int. J. Heat Mass Transfer **124**, 1163 (2018).
[15] S.-H. Lee, S. J. Lee, J. S. Lee, K. Fezzaa, and J. H. Je, Phys. Rev. Fluids **3**, 124308 (2018).
[16] P. Chantelot and D. Lohse, J. Fluid Mech. **928**, A36 (2021).
[17] W. Yuan, T. Wei, and M. Zhang, Int. J. Heat Fluid Flow **95**, 108965 (2022).
[18] M. Adda-Bedia, S. Kumar, F. Lechenault, S. Moulinet, M. Schillaci, and D. Vella, Langmuir **32**, 4179 (2016).
[19] A. Gauthier, C. Diddens, R. Proville, D. Lohse, and D. van der Meer, Proc. Natl. Acad. Sci. U.S.A. **116**, 1174 (2019).
[20] L. Maquet, Ph.D. thesis, Université de Liège (2017), http://hdl.handle.net/2268/204526.
[21] P. G. Kim and H. Stone, Europhys. Lett. **83**, 54001 (2008).
[22] See Supplemental Material at http://link.aps.org/supplemental/10.1103/PhysRevLett.131.184001, which includes Refs. [4,11,13,20,23–30], for details.
[23] Q. Zhou, C. M. Oldenburg, J. Rutqvist, and J. T. Birkholzer, Water Resour. Res. **53**, 9960 (2017).
[24] B. Sobac, L. Maquet, A. Duchesne, H. Machrafi, A. Rednikov, P. Dauby, P. Colinet, and S. Dorbolo, Phys. Rev. Fluids **5**, 062701(R) (2020).
[25] B. Sobac, A. Rednikov, S. Dorbolo, and P. Colinet, Phys. Rev. E **90**, 053011 (2014).
[26] J. Crank, *The Mathematics of Diffusion* (Oxford University Press, New York, NY, 1975).
[27] H. Machrafi, N. Sadoun, A. Rednikov, S. Dehaeck, P. Dauby, and P. Colinet, Microgravity Sci. Technol. **25**, 251 (2013).
[28] D. W. Green and M. Z. Southard, *Perry's Chemical Engineers' Handbook* (McGraw-Hill Education, New York, 2019).
[29] L. I. Stiel and G. Thodos, AIChE J. **10**, 26 (1964).
[30] J. C. Burton, A. L. Sharpe, R. C. A. van der Veen, A. Franco, and S. R. Nagel, Phys. Rev. Lett. **109**, 074301 (2012).
[31] B. Scheid, S. Dorbolo, L. R. Arriaga, and E. Rio, Phys. Rev. Lett. **109**, 264502 (2012).
[32] 3M, Novotec 7100 Engineered fluid, Technical datasheet.
[33] Rhodorsil Oils 47, Bluestar Silicones (2016).